Original article

In silico and in vitro studies on the anti-cancer activity of artemetin, vitexicarpin and penduletin compounds from *Vitex negundo*

Giau Van Vo [a,b,c], Thi-Hoai-Thu Nguyen [d], Thi-Phuong Nguyen [e], Thi-Hong-Tuoi Do [f], Nguyen-Minh-An Tran [g], Huy Truong Nguyen [h,*], Thuy Trang Nguyen [i,*]

[a] Department of Biomedical Engineering, School of Medicine, Vietnam National University – Ho Chi Minh City (VNU-HCM), Ho Chi Minh City 70000, Vietnam
[b] Research Center for Genetics and Reproductive Health (CGRH), School of Medicine, Vietnam National University, Ho Chi Minh City (VNU-HCM), Ho Chi Minh City 70000, Vietnam
[c] Vietnam National University Ho Chi Minh City (VNU-HCM), Ho Chi Minh City 70000, Vietnam
[d] Faculty of Basic Sciences, University of Medicine and Pharmacy at Ho Chi Minh City, 217 Hong Bang Street, Dist. 5, Ho Chi Minh City 72714, Vietnam
[e] NTT Hi-Tech Institute, Nguyen Tat Thanh University, Ho Chi Minh City 70000, Vietnam
[f] Faculty of Pharmacy, University of Medicine and Pharmacy at Ho Chi Minh City, 41 Dinh Tien Hoang Street, Dist. 1, Ho Chi Minh City 72714, Vietnam
[g] Faculty of Chemical Engineering, Industrial University of Ho Chi Minh City, Ho Chi Minh City 71420, Vietnam
[h] Application in Pharmaceutical Sciences Research Group, Faculty of Pharmacy, Ton Duc Thang University, Ho Chi Minh City, Vietnam
[i] Faculty of Pharmacy, HUTECH University, Ho Chi Minh City 70000, Vietnam

ARTICLE INFO

ABSTRACT

Vitex negundo L. (*V. negundo*) is one of the important medicinal and anticancer enhancer herbs. This plant is commonly used in the preparation of traditional drugs to treat numerous diseases. Inspired by the medicinal properties of this plant, the current study aimed to investigate antiproliferative potential and the primary molecular mechanisms of the apoptotic induction against human HepG2 and MCF-7 cell lines, by pure compounds isolated from targeted fractions of *V. negundo* which were characterized by NMR, FTIR and HRMS analysis and identified as artemetin (FLV1), vitexicarpin (FLV2), and penduletin (FLV3) compounds. The FLV1, FLV2, and FLV3 compounds were evaluated for the antiproliferative potential against HepG2 and MCF-7 cell lines by cell viability assay and exhibited IC_{50} values of 2.3, 23.9 and 5.6 μM and 3.9, 25.8, and 6.4 μM, respectively. In addition, those compounds increased the level of reactive oxygen species production, induced cell death occurred via apoptosis, demonstrated by Annexin V-staining cells, contributed significantly to DNA damage, and led to the activation of caspase3/caspase8 pathways.Additionally, molecular docking was also conducted to rationalize the cancer cells inhibitory and to evaluate the ability of the FLV1, FLV2, and FLV3 compounds to be developed as good drug candidates for cancers treatment.

1. Introduction

Cancer is a complicated disease in which cells multiply and grow uncontrollably regards to fifty altered signaling pathways in different tumor types. Cancer cells can be metastasized to the distant parts of the body organs, even after the tumor is completely removed from the primary site (Couffignal et al., 2000). In spite of the enormous efforts and progress in the field of cancer research, the threat of cancer disease is still worsening (Siegel et al., 2022). Chemotherapy, radiotherapy, and surgery are traditional ways that are still considered effective, but due to certain side effects to the normal body cells, some more effective treatment strategies to prevent cancer are need. To minimize these limitations, a large part of chemotherapy agents from natural sources (Newman and Cragg 2016) are demonstrated to be possible candidates and the mechanisms of their action are elucidated (Cragg and Pezzuto 2016). Despite the success of these agents from natural sources, most plant species that have not been systematically investigated in drug discovery campaigns that are still needed to be further explored (Harvey et al., 2015).

* Corresponding authors.
E-mail addresses: nguyentruonghuy@tdtu.edu.vn (H.T. Nguyen), nt.trang85@hutech.edu.vn (T.T. Nguyen).
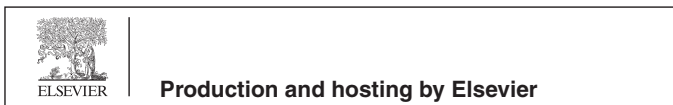
With ∼ 270 species of trees and shrubs the genus *Vitex* is a common plant in temperate zones (Rani and Sharma 2013). Many of them used to treat some common diseases such as rheumatic pains, sprains, respiratory infections, inflammation, anti-cancer, or diuretic (Rani and Sharma 2013). Among that, *Vitex negundo* L. (*V. negundo*) is widely found in Asia countries including Vietnam (Sichaem et al., 2019), exhibited various biological activities due to the presence of phytoconstituents like alkaloids, flavonoids, glycosides, phenols, lignins, saponins, sterols, tannins [8, 9]. Previously, *V. negundo* has been reported to possess various types of pharmacological properties (Díaz et al., 2003, Sathiamoorthy et al., 2007, Gautam et al., 2010), lignans (Zheng et al., 2010), iridoid glycosides (Sharma et al., 2009) and terpenoids (Zheng et al., 2010), some of which exhibited antifungal, antibacterial, anti-inflammatory, antioxidant and anticancer activities (Zheng et al., 2010, Kadir et al., 2013). Our recent study also isolated several labdane-type diterpenoids from on from the leaves of *V. negundo* such as such as vitexnegundin, vitexilactone, vitetrifolin D, and artemetin, vitexicarpin, and penduletin compounds (Sichaem et al., 2019) that could inhibit the growh of malignant cell lines, namely K562 (Li et al., 2005), Lu1, KB, and LNCaP (Díaz et al., 2003). However, their cytotoxicity against breast and liver cancers has not been described yet.

The present study aimed to isolate and further report the phytoconstituent(s) responsible for the anticancer potential from V. negundo. Artemetin (FLV1), vitexicarpin (FLV2), and penduletin (FLV3) compounds were isolated, identified, structured and investigated their cytotoxic, apoptosis induction, and molecular docking activities on human hepatocellular carcinoma (HepG2) and breast cancer (MCF-7) cells.

2. Materials and methods

2.1. Plant procurement, identification and authentication of plant material

The plant *V. negundo* L, with accession no. UP-010, was purchased from the Phu Quy Island, Vietnam (Aug-Nov 2020) associated to Tay Do University, Can Tho, Vietnam and deposited in the herbarium of the Department of Organic Chemistry, Faculty of Chemistry, Ho Chi Minh University of Education, Ho Chi Minh City, Vietnam.

2.2. Experimental procedures

^{1}H and ^{13}C NMR spectra were recorded on Bruker Avance NMR 500 MHz instruments using $CDCl_3$ and DMSO d_6 as deuterated solvents. Chemical shift in ppm was measured relative to TMS as internal standard and coupling constant J was measured in Hz, multiplicity is indicated as: s = singlet, d = doublet, t = triplet, m = multiplets. IR spectra was recorded on Agilent- FT-IR technologies, USA.

2.3. Isolation of fragments and compounds

The plant material was washed with distilled water and kept at 40 °C. The dried plant was coarse grinded (7 kg) and soaked in 20 L × 3 ethyl acetate for 12 h at ambient temperature. Further, fractionation was performed using different organic solvents with increasing polarity, viz. hexane to yield 0.75 kg EtOAc crude extract, *n*-hexane and *n*-hexane-EtOAc (1:1, v/v), and EtOAc, to yield 175 g, **H (**yielding *n*-hexane), 35 g, **HEA** (*n*-hexane-EtOAc (1:1)), and 340 g, **EA** (EtOAc) extracts, respectively. Following our previous study (Sichaem et al., 2019) with some modifications, 35 g **HEA** extract was then subjected to Sephadex LH-20 gel

chromatography and finally eluted with methanol to obtain **HEA1-4** fraction. A 3.5 g **HEA4** was continuously purified using silica gel column chromatography (CC) in *n*-hexane-EtOAc-acetone (20:1:1, v/v/v) to provide **HEA4.1–3** fraction. A 701 mg **HEA4.3** was process to preparative thin-layer chromatography, and eluted with the solvent system of *n*-hexane-EtOAc-chloroform-acetic acid (30:10:10:0.01, v/v/v/v), to final obtaining compounds including 35 mg **FLV1**, 12 mg **FLV2**, and 5.1 mg **FLV3**.

2.4. Sreening bioactive compounds

In order to screening crude extracts and fractions for the presence of bioactive compounds, the MTT assay was used as previously reported (Duong et al., 2017). Briefly, 10^4 HepG2 cells/100 μL/well inoculated in 96-well plate and maintained at 37 °C and 5% CO_2 with 95% humidity for 24 h. Then, the cells were treated with the compounds and doxorubicin (positive control) diluted in culture media at various concentration. The plates were further incubated for 48 h. 10 μL of 3-(4,5-dimethylthiazol-2-yl)-2,5- diphenyltetrazolium bromide (MTT, 5 mg/ml stock solution) was added into each well and incubated in 37 °C in 5% CO_2 for 3.5 h, followed by adding 70 μL of Detergent Reagent (10% SDS)/well and cultured further in 37 °C for 16 h. The cell survival was finally measured at wavelength of 595 nm using a scanning multi-wall spectrophotometer (Sunrise).

2.5. Cell viability evaluation

Cell viability evaluation was done as previously described (Nguyen et al., 2020). Briefly, the HepG2 and MCF-7 cells line were seeded in a 96-well plates at 5×10^4 cells/well then followed by treating with FLV1, FLV2, FLV3, or Doxorubicin (Dox) as positive control at concentration range of 0 and 100 μM. After 48 h, 100 μL fresh medium was replaced and 100 μL of CellTiter-Glo® Luminescent reagent (Promega, Madison, WI, USA) added. The cell viability was finally measured and viability percentage was calculated in comparing the control groups.

2.6. Determination of intracellular ROS generation

The changes in ROS generation after treatment with compounds in the HepG2 and MCF-7 cells were evaluated according to the ROS assay kit (ab113851, Abcam) instructions. Briefly, the cells (4×10^5 cells/well) were cultured for 24 h in a six-well plate followed by the IC_{50} concentration of compounds. After 24 hr, DCFH-DA (5 μM) was added to the cells and incubated for 45 min at 37 °C in protection from light, followed by washed with PBS and finally measured the fluoresces intensity. Tert-butyl hydrogen peroxide (TBHP) was used as positive control to mimic ROS activity to oxidize DCFDA to fluorescent DCF.

2.7. Flow cytometry assays

An Annexin V-FITC/Propidium iodide (PI) binding assay kit was used to determine inducing of apoptosis in the cells (Thermo Fisher Scientific, CA, USA). After treatment, the cells were analyzed by flow cytometry to determine the percentages of cell apoptotic distribution using FlowJo software (version 10.7.1).

2.8. The assessment of DNA fragmentation

To further uncover apoptosis, the cells were treated with FLV1, FLV2 or FLV3 at the IC_{50} doses. After 24 h incubation, total DNA was carefully isolated using DNA purification kit (Thermo Fisher Scientific, Santa Clara, CA, USA) and analyzed in electrophoresis with

Table 1
Cytotoxic effects of isolated Vitex negundo extracts against human cancer cells studied by MTT assay.

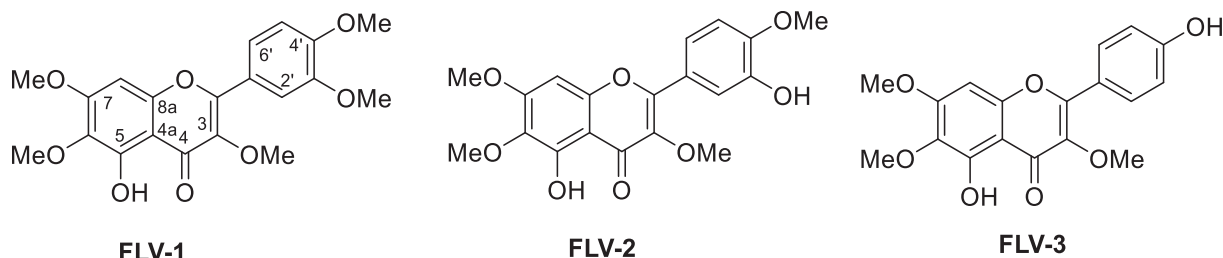| Samples	Crude extract	Extract HEA	Extract H	Extract EA	DOX
IC_{50} (µg/mL)	55.56 ± 1.1	37.02 ± 4.21	45.21 ± 2.87	> 100	4.51 ± 0.05

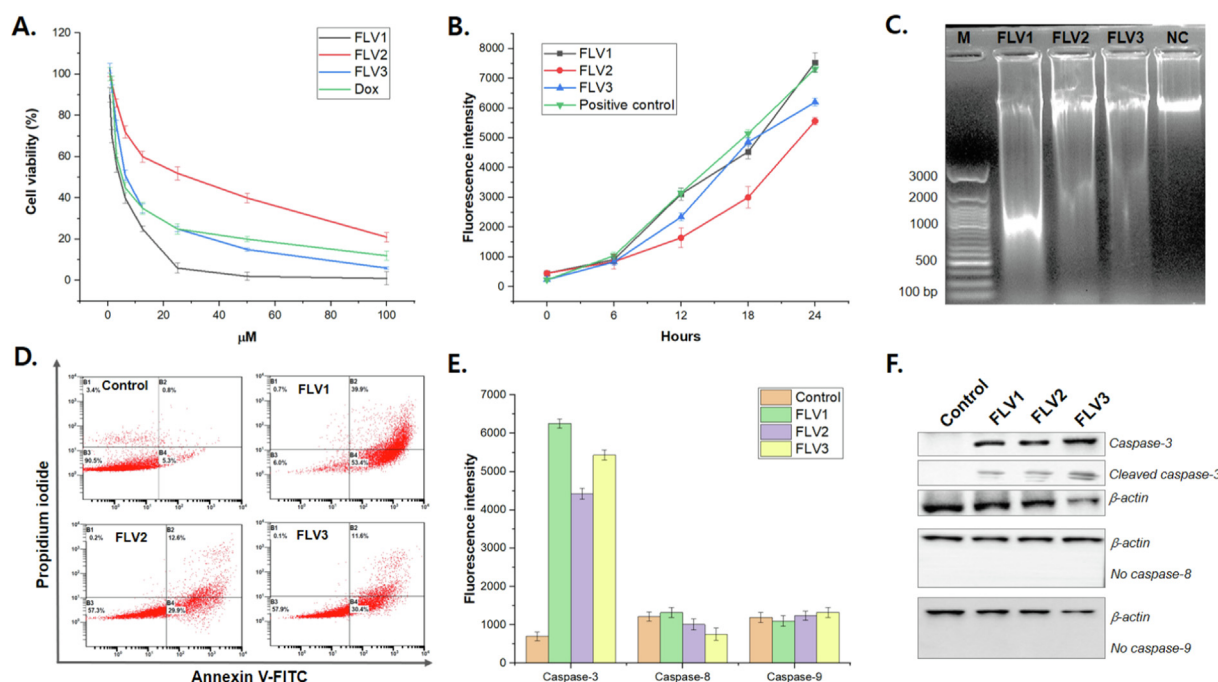**Fig. 1.** FLV1, FLV2 and FLV3 structures.

Fig. 2. Evaluation of anticancer effect and investigating apoptotic effects of FLV1, FLV2 and FLV3 compounds on HepG2 cells. **A.** Cell viability; **B.** ROS production; **C.** DNA fragmentation; **E.** Quantification of apoptosis; **D.** Caspase activities screening and **F.** Western-blotting verification.

1.5% agarose gel to evaluate the DNA fragmentation as previously described (Shaker and Melake 2012).

2.9. Detection of active caspases

The caspase 3/8/9 activities assay kit (Abcam, Cambridge, UK) was used to further evaluate fundamental mechanism of apoptosis as the manufacturer's introductions. Briefly, 2×10^4 cells/well on 96-well plates was treated with FLV1, FLV2, FLV3 compounds at its IC_{50} dose, followed by adding 100 µL of caspase reagent after 24 h incubation. The caspase-3, −8, and −9 activities were finally measured as fluorescence intensity of each well.

2.10. Western bloting

The expression levels of proteins involved directly in the cell apoptotic proteins (caspase3-8–9) were analyzed by Western blotting. Firstly, the cells (5×10^6) were cultured and treated with each compounds (IC_{50} dose) for 24 hr. The cells were col-

lected using a cell scraper and cell pellet was obtained by centrifugation at 1500 rpm for 5 min. For cell lysis, 150 µL of RIPA buffer was added to the cell pellet and kept on ice for 25 min then centrifuged for 25 min, supernatant was collected and protein concentration was quantified by Bradford method. Equal amount of protein (40 µg) from compounds treated and untreated cells was resolved by SDS-PAGE and was transferred to Polyvinylidene difluoride (PVDF) membrane using a wet transfer apparatus (Biorad, CA, US). After that, the PVDF membrane was blocked using BSA (5% in TBST, 0.1 % Tween-20) for 2 h at RT and overnight incubated with primary antibodies caspase3/8/9 (1:1,500) at 4 °C. The membrane was washed thrice with TBST and HRP-conjugated secondary antibody (1:1,500) was added and the membrane was incubated for 2 h at room temperature. The blot was imaged under Image-Quant LAS 4000, GE 13 Healthcare. Band densities were quantified with Alphaease 258 FC Software (version 4.0). β-actin (1:1,500) as endogenous control was used for stabilizing the expression of the protein of interest.
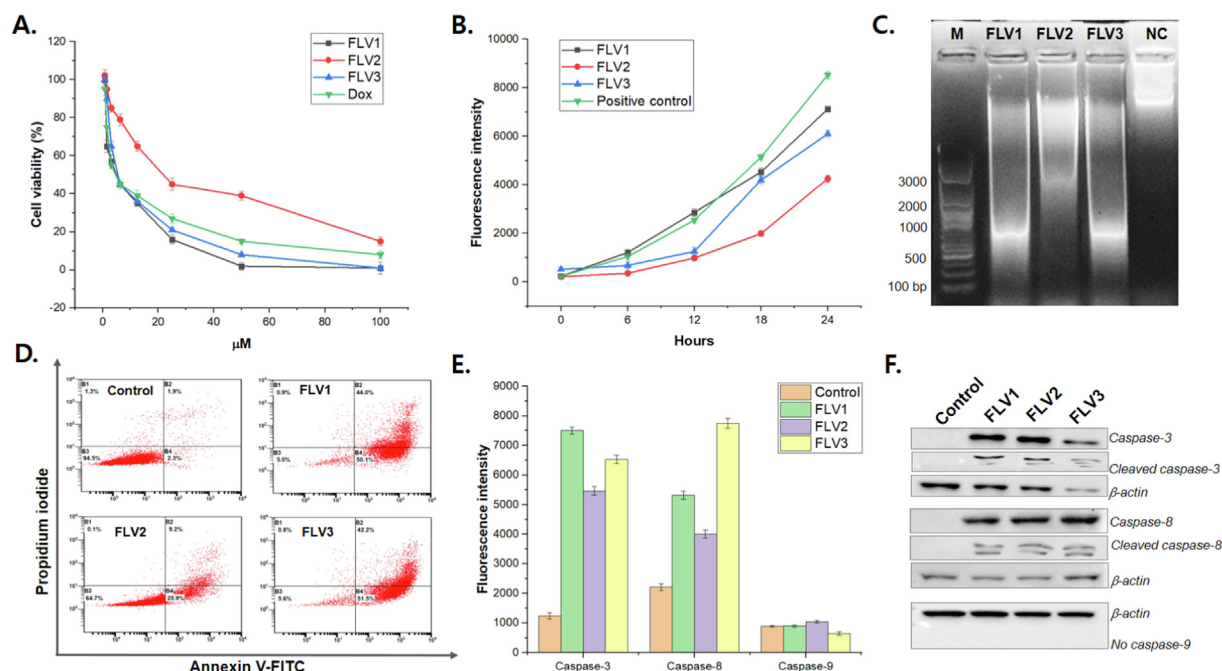
Fig. 3. Evaluation of anticancer effect and investigating apoptotic effects of FLV1, FLV2 and FLV3 compounds on MCF-7 cells. **A.** Cell viability; **B.** ROS production; **C.** DNA fragmentation; **E**. Quantification of apoptosis; **D.** Caspase activities screening and **F.** Western-blotting verification.

2.11. Molecular docking study method

To predict drug-receptor interactions, the molecular docking model were performed as our previous studies (An et al., 2020, Duong et al., 2020) and briefly described bellow in **Scheme S1** from **Supplemental file**. For MCF-7 and Hep-G2 cells, *in silio* docking, we used **7KCD and 2G33: PDB code,** respectively and the active center of every PDB was additionally determined at coordinates of (X = **14.607, Y = -8.635, Z = 41.992) for 7KCD** and (X = **197.6150, Y = 95.458, Z = 127.433)** for 2G33. The grid parameters set up in dock.gpf file as spacing of 0.5 Å and the numbers of elements of X = 60, Y = 60 and Z = 60) with receptor 7KCD and 2G33. The input and output of docking parameters are genetic algorithm and Lamarckian, respectively with 400 models, which was performed. The validations of model are calculated based on the values of RMSD (Bell and Zhang 2019, Sibanyoni et al., 2020).

2.12. Statistical analysis

One-way analysis of variance ANOVA was used to calculate statistical significance of all the values. The difference among the means was further compared by high-range statistical domain (HSD) using Tukey's test. For all the experiments, the values were represented as Mean ± standard errors (SE) in triplicate values. The probability $p \leq 0.05$ was used to demonstrate that all the values were statistically significant at a 5% level.

3. Results

3.1. MTT viability assays for electivity studies

Table 1 showed that from the selected four extracts and fractions, only three had potential cytotoxicity with the IC$_{50}$ values<60 µg/ mL. Notably, the HEA fraction of *V. negundo* had the highest cytotoxicity on HepG2 cell line, with a IC$_{50}$ value of 37.02 ± 4.21 µg/mL, compared to doxorubicin (Dox) (IC$_{50}$ value ∼ 4.51

± 0.05 µg/mL). The HEA fraction was selected for further studies based on its cytotoxic activities.

3.2. Identification of artemetin, vitexicarpin and penduletin

Compound FLV1 (Fig. 1): Light yellow amorphous powder. ^{1}-HNMR (500 MHz, DMS0-d_6): δ 12.53 (1H, *s*, 5-OH), 7.69 (1H, *dd*, *J* = 2.0, 8.5 Hz, H-6′), 7.61 (1H, *d*, *J* = 2.0 Hz, H-2′), 7.11 (1H, *d*, *J* = 8.5 Hz, H-5′), 6.89 (1H, *s*, H-8), 3.88 (6-OCH$_3$), 3.82 (7-OCH$_3$), 3.81 (3′-OCH$_3$), 3.77 (3-OCH$_3$), 3.68 (4′-OCH$_3$). ^{13}CNMR (125 MHz, DMS0-d_6): δ 178.4 (C-4), 158.8 (C-7), 155.6 (C-2), 151.9 (C-5), 151.7 (C-8a), 151.4 (C-4′), 148.7 (C-3′), 138.1 (C-3), 131.7 (C-6), 124.0 (C-2′), 122.2 (C-1′), 111.7 (C-6′), 111.3 (C-5′), 105.7 (C-4a), 91.6 (C-8), 60.1 (7-0CH$_3$), 56.6 (3-0CH$_3$), 55.8 (6-0CH$_3$), 55.8 (3′-0CH$_3$), 55.7 (4′-0CH$_3$). The finding was artemetin (Azhar Ul et al., 2004). 1D NMR spectra of FLV1 were provided in Fig. S1-2.

Compound FLV2 (Fig. 1): Light yellow amorphous powder. ^{1}H NMR (500 MHz, DMSO d_6): δ 12.60 (1H, *s*, 5-OH), 9.42 (1H, *s*, 3′-OH), 7.59 (1H, *dd*, *J* = 2.0, 9.0 Hz, H-6′), 7.58 (1H, *d*, *J* = 2.5 Hz, H-2′), 7.12 (1H, *d*, *J* = 9.0 Hz, H-5′), 6.88 (1H, *s*, H-8), 3.93 (7-OCH$_3$), 3.88 (6-OCH$_3$), 3.82 (3-OCH$_3$), 3.75 (4′-OCH$_3$). ^{13}C NMR (125 MHz, DMSO d_6): δ 178.3 (C-4), 158.7 (C-7), 155.6 (C-2), 151.8 (C-5), 151.7 (C-8a), 150.3 (C-4′), 146.4 (C-3′), 138.0 (C-3), 131.6 (C-6), 122.2 (C-2′), 120.4 (C-1′), 112.0 (C-6′), 105.6 (C-5′), 105.6 (C-4a), 91.3 (C-8), 60.0 (7-0CH$_3$), 59.7 (3-0CH$_3$), 56.5 (6-OCH$_3$), 55.7 (4′-OCH$_3$). The data were consistent and suggested to be vitexicarpin [1]. 1D NMR spectra of FLV2 were further indicated in Fig. S3-4.

Compound FLV3 (Fig. 1): Light yellow amorphous powder. ^{1}H NMR (500 MHz, chloroform-*d*): δ 12.61 (1H, *s*, 5-OH), 8.04 (2H, *d*, *J* = 8.5 Hz, H-2′,6′), 6.97 (2H, *d*, *J* = 8.5 Hz, H-3′,5′), 6.50 (1H, *s*, H-8), 3.96 (7-OCH$_3$), 3.93 (6-OCH$_3$), 3.86 (3-OCH$_3$). ^{13}C NMR (125 MHz, chloroform-*d*): δ 178.9 (C-4), 159.0 (C-4′), 158.2 (C-7), 156.1 (C-2), 152.9 (C-8a), 152.4 (C-5), 138.8 (C-3), 132.3 (C-6), 130.2 (C-6′), 130.2 (C-2′), 123.1 (C-1′), 115.7 (C-5′), 115.7 (C-3′),

106.8 (C-4a), 90.5 (C-8), 61.1 (3-OCH$_3$), 60.3 (6-OCH$_3$), 56.5 (7-0CH$_3$). The finding was penduletin (Zheng et al., 2009). 1D NMR were further provided in Fig. S5-6.

3.3. Cytotoxic effect of FLV1, FLV2 and FLV3 in liver and breast cancer cells proliferation

In the current study, the cytotoxicity of FLV1, FLV2 and FLV3 were evaluated using the cell viability assay in both HepG2 and MCF-7 cells lines exposed to ranging 0–100 μg/mL of the compounds for 48 h incubation. Cell viability analyses revealed that FLV1, FLV2 and FLV3 caused development inhibition of HepG2, and MCF-7 cell lines in dose-dependent manners (Fig. 2A and Fig. 3A). FLV1, FLV2 and FLV3 were found to have an excellent cytotoxic effect on HepG2 cells with a IC$_{50}$ value of 2.3 ± 0.6, 23.9 ± 0.6 and 5.6 ± 0.7 μM, respectively (Fig. 2A). Notably, compounds FLV1 and FLV3 revealed more cytotoxic activity for HepG2 cells than that of FLV2 in terms of IC$_{50}$ with same concentration. However, the compounds FLV1 and FLV3 notably exhibited to have excellent cytotoxic activity with an IC$_{50}$ value

of 6.0 μM for HepG2 cells. Similar figures were observed for FLV1, FLV2 and FLV3 against MCF-7 cells with the IC$_{50}$ values of 3.9 ± 0.6, 25.8 ± 0.9, and 6.4 ± 1.26 μM respectively as shown in Fig. 3A. Similar trends were also received for Dox with IC$_{50}$ values of 2.6 ± 0.32 μM and 4.2 ± 0.28 μM for HepG2 and MCF-7 (p < 0.01), respectively. Although FLV2 was slightly less effective than FLV1 and FLV3 due to its IC$_{50}$ values of 23.9 ± 0.6 μg/mL and 25.8 ± 0.9 μM for HepG2 and MCF-7 cell lines, respectively, indicating that FLV1, FLV2 and FLV3 excellent exhibited highly cytotoxic effects against HepG2 and MCF-7 cells (Goldin et al., 1981, Grever et al., 1992). In contrast to the two cancer cell lines tested, while the non-cancer-derived cell line HEK293 exhibited high sensitivity to Dox under the same conditions (IC$_{50}$ = 0.98 μM), minimal cytotoxicity was observed for FLV1, FLV2, and FLV3 (IC$_{50}$ was not reached even at the highest concentrations of tested) (Figure S7). The present results strongly confirmed that FLV1, FLV2 and FLV3 compounds could be highly active and extremely potent as anticancer agents against the two cancer cell lines.
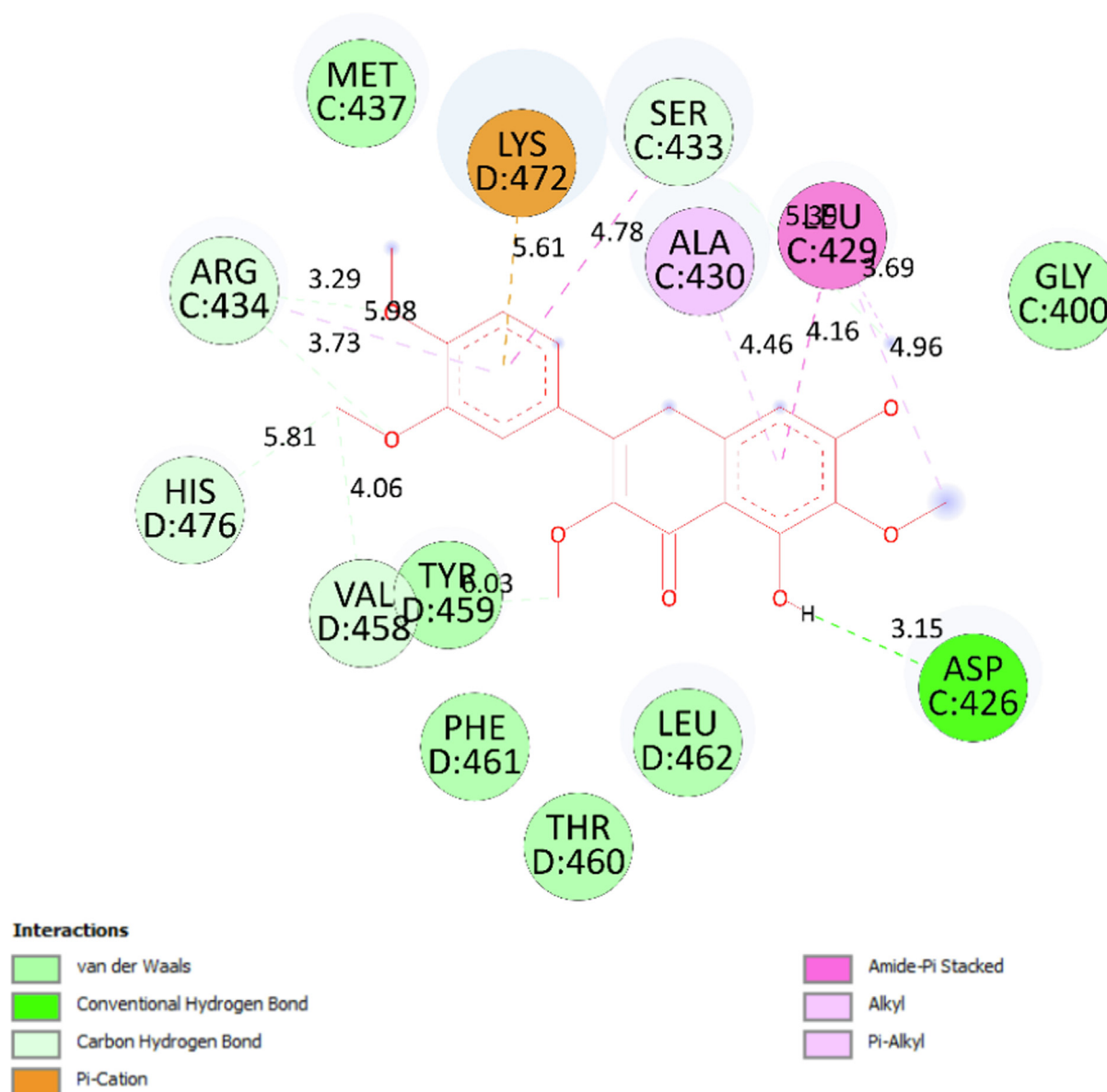

Fig. 4. The significant ligand interactions between ranked pose 35, ranked pose of ligand FLV-1 and 7KCD: PDB code.
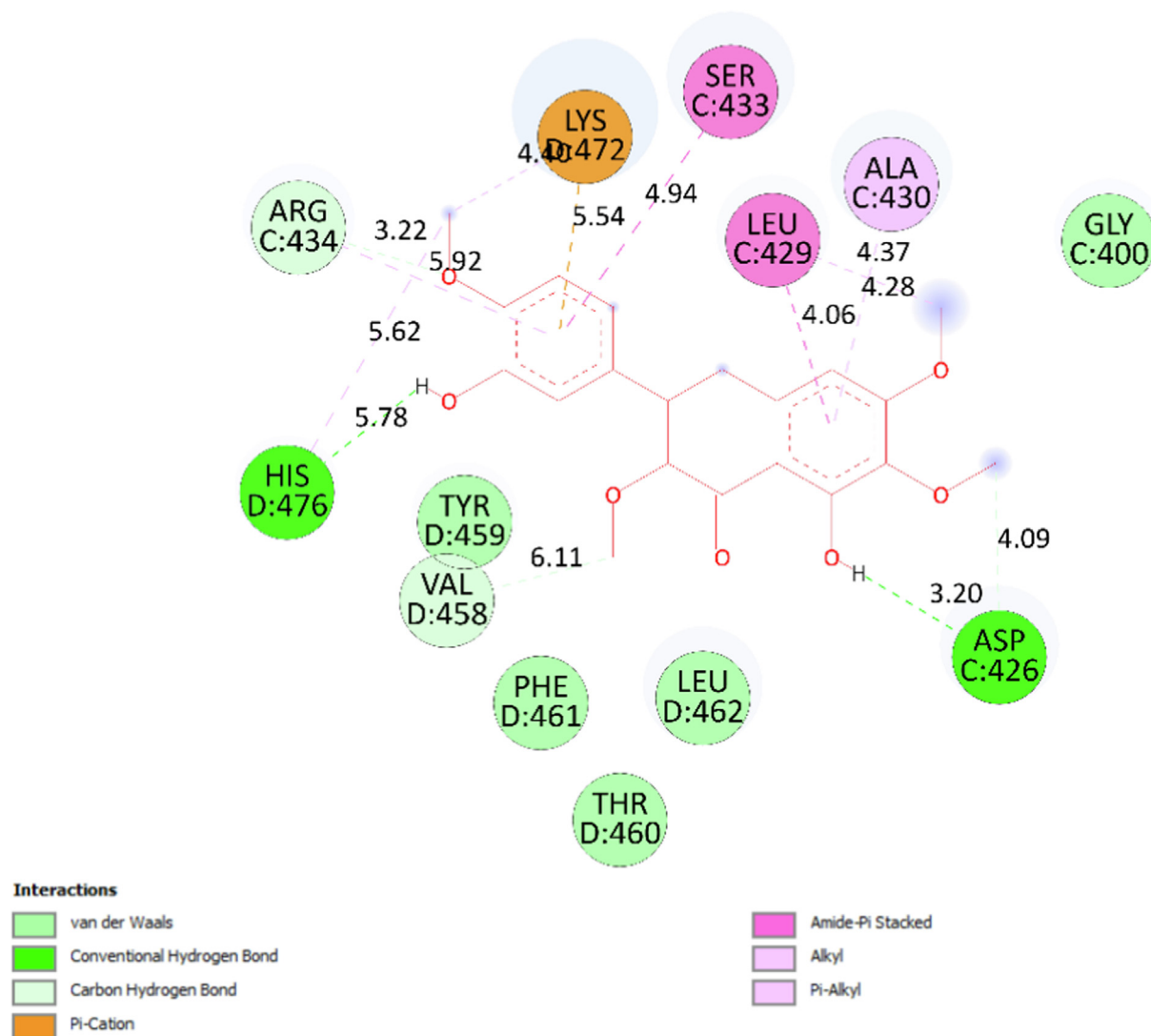
Fig. 5. The significant ligand interactions between ranked pose 375, ligand FLV-2 and 7KCD: PDB code on one 2D diagram.

3.4. Investigating apoptotic effects of FLV1, FLV2 and FLV3 compounds

ROS play a significant role in apoptosis and mitochondrial-mediated pathway (Kumar et al., 2015). ROS generation was further observed by DCFH-DA probe that is deacetylated by cell esterase enzyme and oxidized by ROS into the fluorescent 2′,7′-dichlorofluorescein (DCF) (Postiglione and Muday 2020). An increase in DCF fluorescence was observed when after exposure of HepG2 and MCF-7 cells to those compounds at IC50 concentration in time-dependent. Time-dependent ROS generation by FLV1, FLV2 and FLV3 on HepG2 and MCF-7 cells were shown in Fig. 2B and Fig. 3B respectively. There were significant increases in the DCF fluorescence for at least 8 h following treatment on HepG2 cells (Fig. 2B), while these figures had little effect on intracellular oxidation from 0 to 6 h. Similarly, intracellular ROS release did not significantly differ from 0 to 8 h of incubation with FLV1, FLV2 and FLV3 compounds (p < 0.05), whereas there was significant increase in the DCF fluorescence for at least 12 h following treatment (p < 0.05) on MCF-7 cells (Fig. 3B). Consequently, FLV1, FLV2 and FLV3 could induce apoptosis in the cancer cells through ROS generation enhanced, and these effects may be evaluated in different ways in case of cell types, compounds, and incubation times.

In order to determine the initial mechanism of cell death mediatedby FLV1, FLV2 and FLV3, we further performed DNA fragmentation assay, which is characteristic for apoptosis.. The HepG2 and MCF-7 cells were treated with FLV1, FLV2 and FLV3 at IC50 concentration, further incubated for 24 h; and DNA was then isolated and analyzed by 1.5% agarose gel electrophoresis. As Fig. 2C and Fig. 3C revealed that HepG2 and MCF-7 cells treated with FLV1, FLV2 and FLV3 at their IC50, a typical ladder pattern of internucleosomal fragmentation were observed after only 24 h incubation, respectively. These data suggest that FLV1, FLV2 and FLV3 were potent inducers of apoptosis in these cells.

In addition, to additional investigate the possible induction of cell death an assessment of apoptosis by Annexin V/PI on the cancer cells was additional investigated. After treatment, the HepG2 and MCF-7 cells were harvested and apoptosis was examined by flow cytometry as revealed on Fig. 2D and Fig. 3D, respectively. Untreated groups showed the percentages of the apoptotic cells were to be 6% and 12% for HepG2 and MCF-7 cells after 24 h incubation (Fig. 2D; Fig. 3D). Apoptosis induced by 23 μM ($\sim$IC$_{50}$) of FLV2 was significantly greater than in untreated cells and the percentage of early and late apoptotic HepG2 cells were $\sim$ 42.5% while the control cells just were $\sim$ 8.1% (Fig. 2D), these figures were found to be similar for MCF-7 cells (Fig. 3D). Remarkably, the pro-
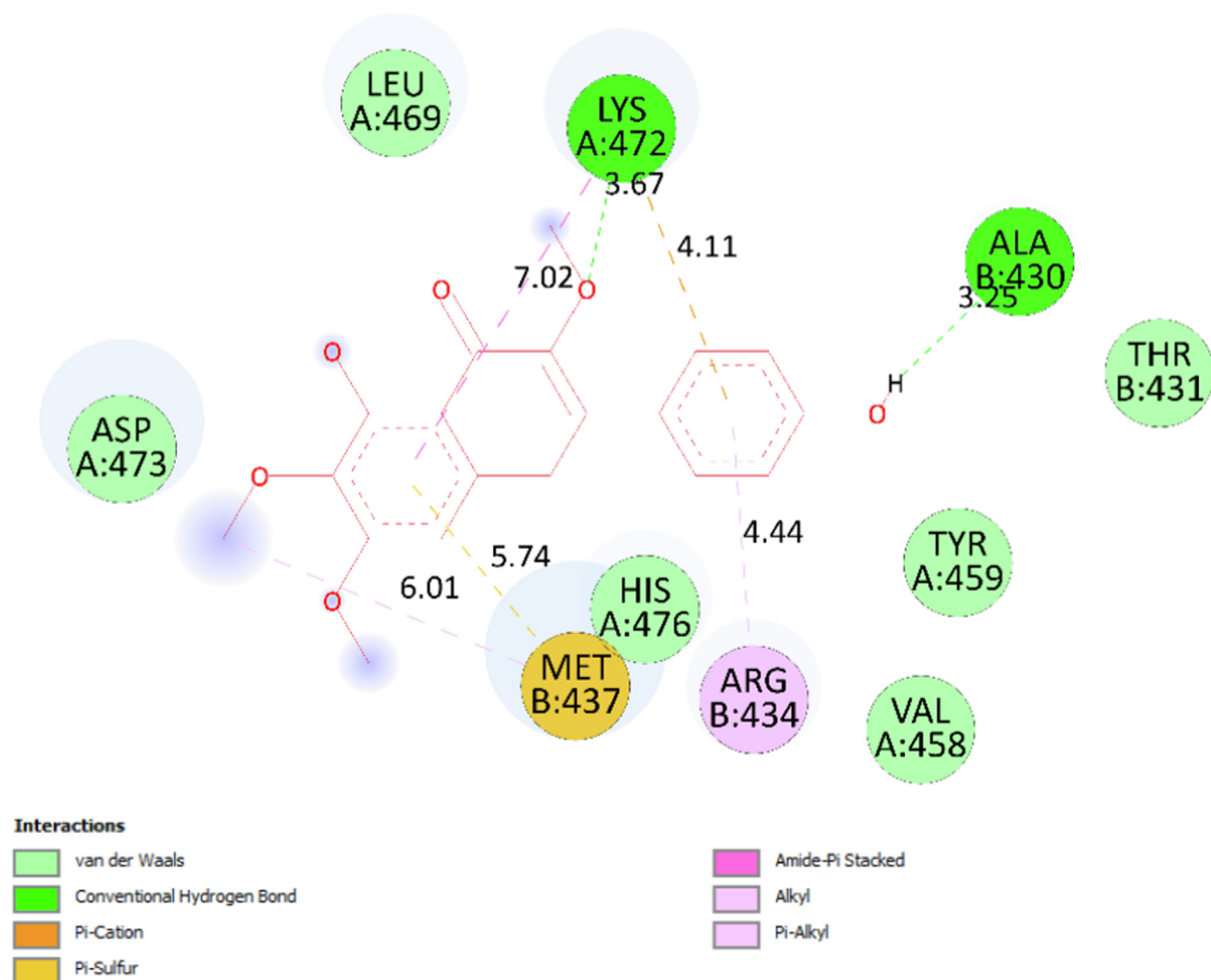
Fig. 6. The significant ligand interactions between ranked pose 23, one ranked pose of ligand FLV-3 and 7KCD: PDB code on one 2D diagram.

portion of apoptosis and necrosis increased significantly with FLV1 and FLV3 treaments. In addition, treatment with the FLV1 at 2 μM resulted in viable (57.9%), early apoptotic (0.1%), late apoptotic (11.6%), and dead cell populations (30.4%) on HepG2 cells (Fig. 2D**)**, while the respective values were 5.0%, 0.9%, 44.0%, and 50.1% for MCF-7 cells after exposing at 4 μM (Fig. 3D). Remarkably, FLV3 exhibited the highest induction of total apoptosis, 20.41-fold and 28.21-fold greater than that of negative control HepG2 and MCF-7 cells respectively.

Given their involvement in apoptosis, caspases and their enzymatic activities are often used as biomarkers for that process (Fulda and Debatin 2006). Hence, we further studied the mechanism of the caspase-3/8/9 activities. As indicated in Fig. 2E, the exposure of HepG2 cells to the FLV1, FLV2 and FLV3 were able to activate caspase-3, while there was no significant change in caspase-8 and 9 activities compared to the control groups. IHepG2 cells treated with FLV1, FLV2, and FLV3 compounds at their IC_{50} doses resulted in a significant increase of caspase-3 activities by roundly 10, 8, and 9-fold compared to untreated cells, respectively. On the other hand, compounds FLV1, FLV2, and FLV3 displayed a remarkable significant increase in the activity of both caspase-3 and −8 on MCF-7 cells(Fig. 3E). In contrast to HepG2 cells, caspase-8 was only activated in MCF-7 cells by 8, 6, and 7-fold after treatment with FLV1, FLV2, and FLV3 compounds, respectively (Fig. 3E).

In order to further confirm whether the changes in expression of apoptosis-related caspase-3, −8, and −9 proteins induced by FLV1, FLV2, and FLV3 compounds at their IC_{50} doses, we measured protein expression in HepG2 and MCF-7 cells after 24-h treatment by the immunoblotting. As indicated in Fig. 2F, caspase-3 protein was upregulated in HepG2 cells in comparison to the untreated control cells. Addition to an activated caspase-3/-8 were upregulated in compounds-treated MCF-7, but not from compound-untreated as shows in Fig. 3F. Consistent with the fluorescence intensity measurement (Fig. 2D and 3D**)**, FLV1, FLV2 and FLV3 exhibited an enhanced ability to induce the cleavage of procaspase-3 in HepG2 and both procaspase-3 and procaspase-8 in MCF-7 cells line in compared to untreated groups, respectively. Conclusively, these results demonstrate that FLV1, FLV2, and FLV3 were effective growth inhibition of the cancer cells by activating procaspase-3 (liver and breast) and procaspase-8 (breast).

Docking of ligand FLV-1 to FLV-3 and drug, DOX to receptor 7KCD Molecular docking is widely used in design and discovery of drugs to enhanced understand the drug-receptor interaction as well as gene pathway (Enkhtaivan et al., 2017). A molecular docking model of three compounds regards their cytotoxicity on two cancer cell lines was conducted. The significant interaction profiles of ligand interactions between FLV-1, FLV-2, FLV-3, DOX (standard drug) and receptor: **7KCD or 2G33**: PDB file and validation method have shown in Figs. 4-13 (building of role docking results**)**, and
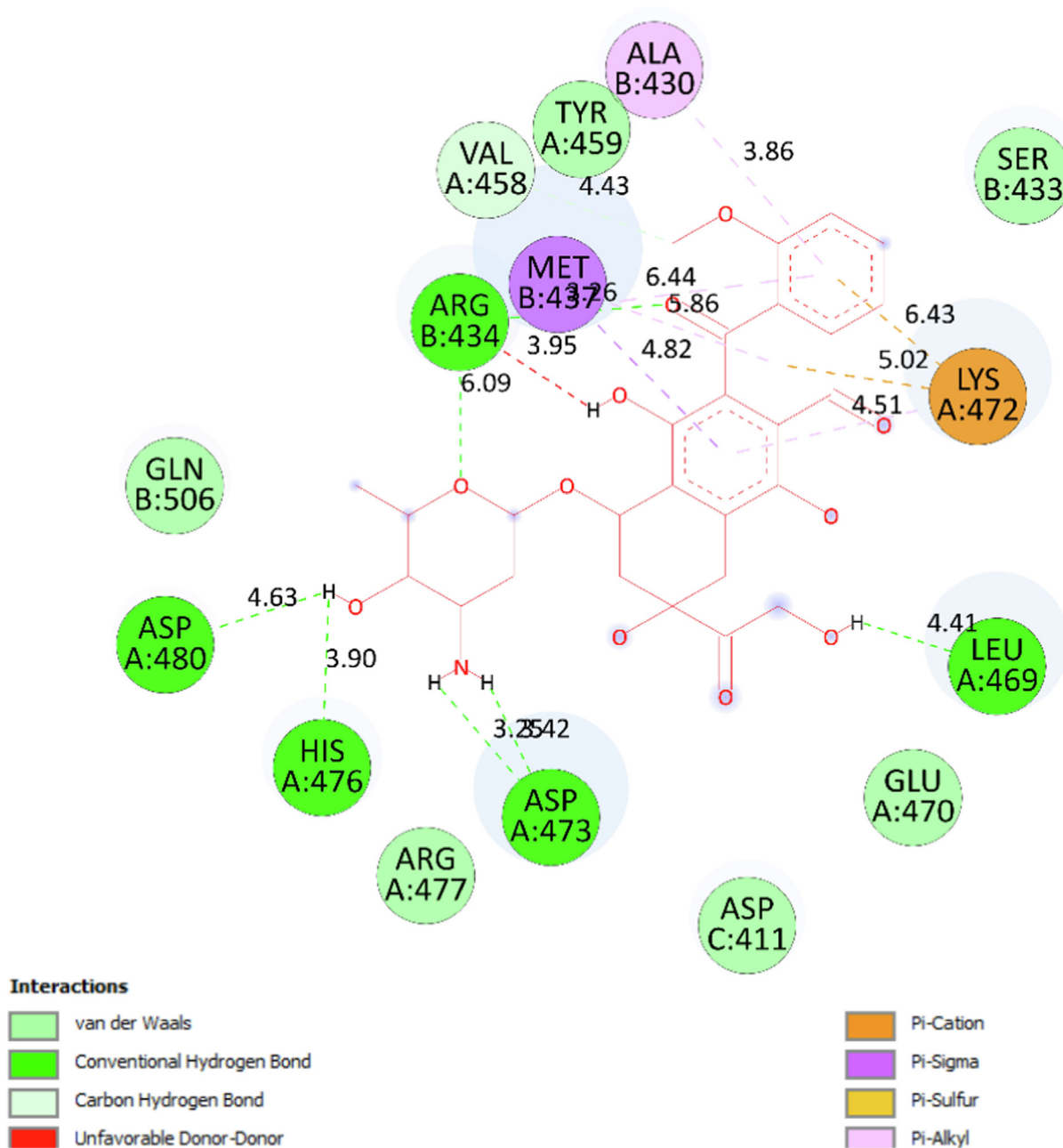
Fig. 7. The significant ligand interactions between ranked pose 139, one ranked pose of ligand DOX and 7KCD: PDB code on one 2D diagram.

Table 2-4 (the values of RMSD between pair poses). For the cells, receptor 7KCD: PDB are used to explain the anticancer in *silico* molecular docking model. In *silico* molecular docking model revealed FLV-2 and FLV-3 are the best candidates docked to 7KCD and 2G33, receptively.

4. Discussion

With 10 million deaths in 2020, cancer is a leading cause of death worldwide and figures show its incidence is continuously increasing (Sung et al., 2021). Despite of great advancements are developed in drugs for cancer treatment; it still has so much more room for improvement. Numerous natural compounds have shown the potential of altering the cellular signaling pathways due to their antioxidant, anti-metastatic, pro-apoptotic and anti-

proliferative properties (Rajora et al., 2020). Herbal remedy recipes are rich sources of phytochemicals enabling guidance for potential drug-leads (Cragg and Newman 2013). These natural compounds specifically halt the progress of carcinogenesis by repairing DNA damage and reducing inflammation (Desai et al., 2008) which may reduce adverse side effects.

In this study, the potential anticancer and mechanisms properties of compounds FLV1, FLV2 and FLV3 from *Vitex negundo* in Vietnam that were demonstrated. Cytotoxicity results revealed that compound FLV1 at concentrations of 2.3 and 3.9 μM had a significant cytotoxic against HepG2 and MCF-7 cells, respectively. While compound FLV3 exhibited excellent inhibition against HepG2 and MCF-7 to be 5.6 and 6.4 μM, respectively. Given the important role that caspases such as caspase-3, −8, and −9 play in destroying the cell during the apoptosis process, their activation and subsequent
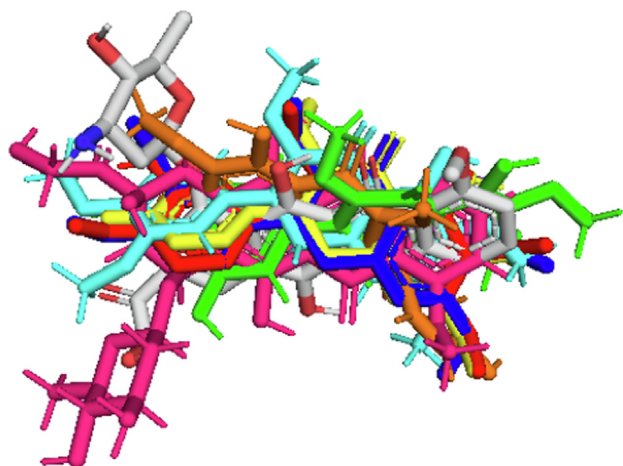
Fig. 8. Pose 35 (blue color), pose 23 (yellow), pose 139 (magenta), FLV-1 (cyan), FLV-2 (green), FLV-3 (orange), and Doxobusin (hot pink) aligned to Pose 375 (red color).

activities are strictly regulated (Brentnall et al., 2013, Wu et al., 2016). By fluorescence intensity revealed caspase-3, −8 activities in MCF-7 cells treated with of compounds FLV1-3 for 24 h whereas caspase-3 cascade is only observed in HepG2 cells. Fig. 3E strongly demonstrated that caspase-3 and −8 remarkably have significant activation in comparison to other caspase and untreated cells during treatment with FLVs compounds, while casepase-3 is only activated after HepG2 exposed to these compounds as showed on Fig. 2E. The elevation of caspase-3 or caspase-3/8 could be verified apoptosis induction in HepG2 and MCF-7 cells lines, respectively. The expression level of caspase-3 or caspase-3/8 activity elevated in treated cells are clearly confirmed by western blot (Fig. 2F and 3F), resulting in activation of caspase-3 activation and apoptosis. Furthermore, DNA fragmentation results also revealed that DNA damage that may support the activation of the caspase activities via the caspase cascades.

On the other hand, molecular docking is widely used in design and discovery of drugs to enhanced understand the drug-receptor interaction as well as gene pathway (Enkhtaivan et al., 2017). Here, FLV1, FLV2 and FLV3 compounds revealed their putative binding
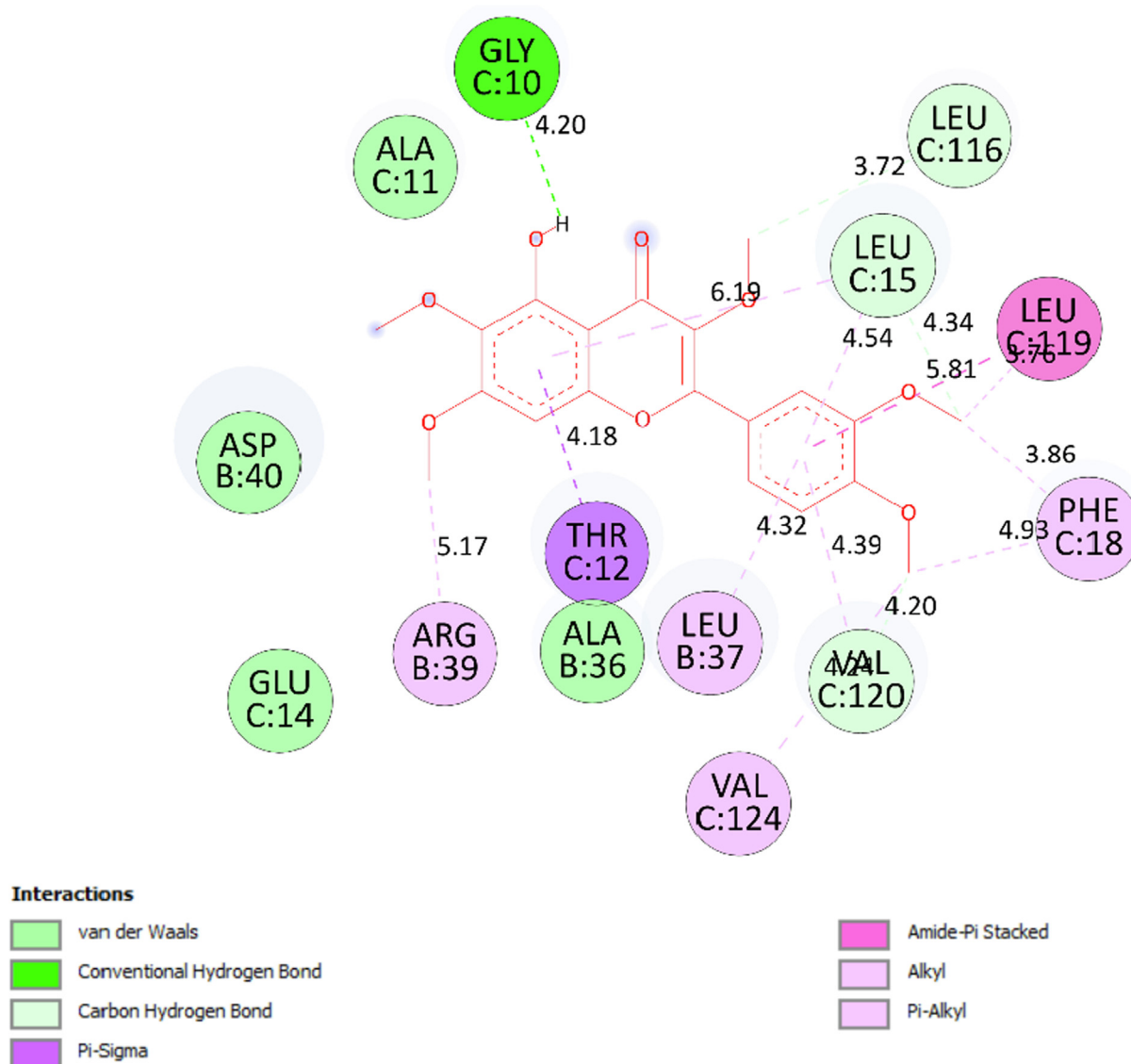

Fig. 9. Pose 85 one ranked pose of ligand FLV-1 was docked to **2G33: PDB.**
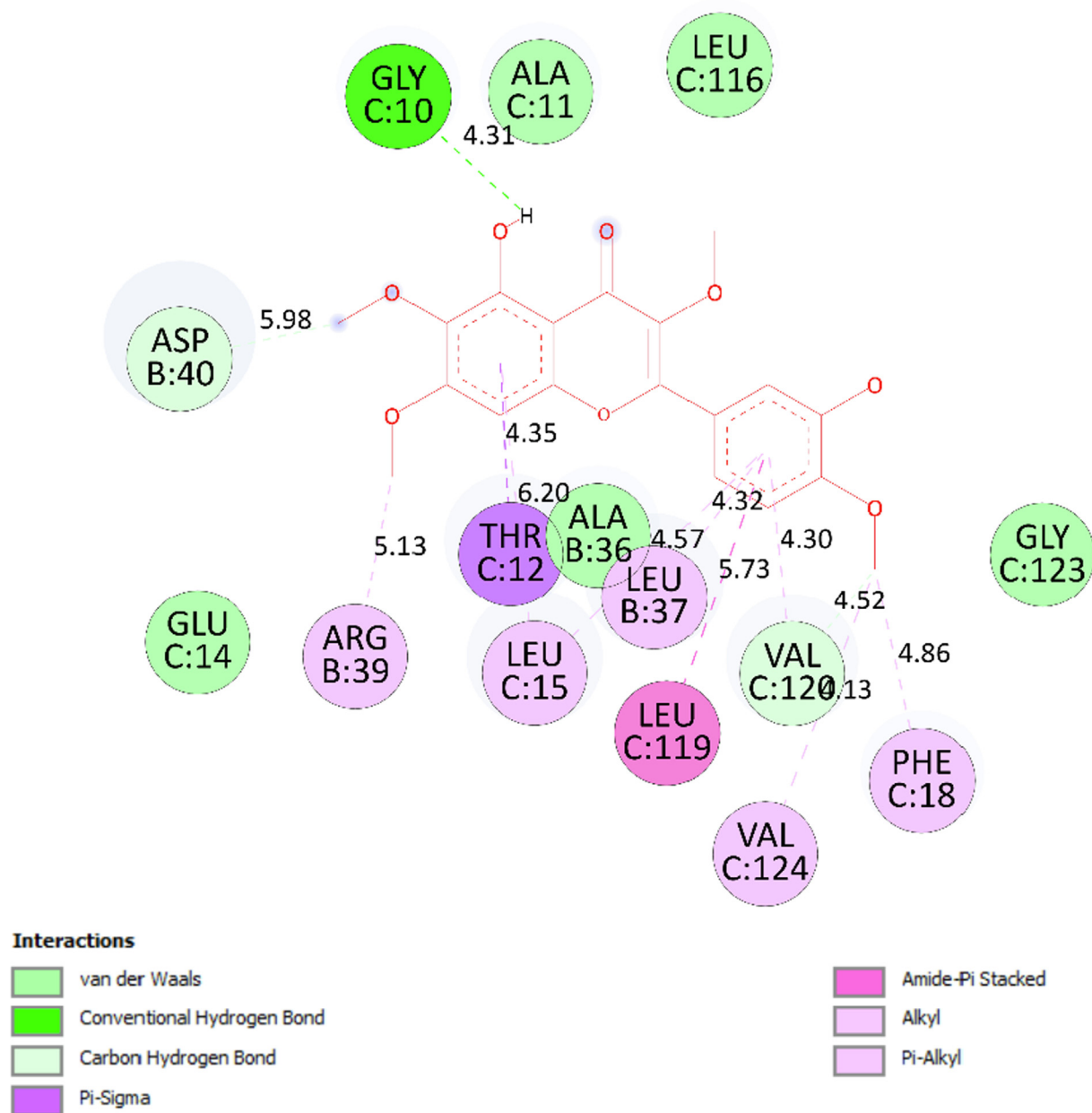
Fig. 10. Pose 88 one ranked pose of ligand FLV-2 was docked to **2G33: PDB.**

mode and significant interactions in docked complex from HepG2 and MCF-7 cell lines as prospective agents for anticancer. The most stable conformation ligand of FLV – 1, pose 35/400 poses has selected and docked to receptor code 7KCD: PDB at active center on 7KCD with the values of the most negative Free Gibbs energy, ΔG^o and the inhibition constant, K_i of -7.71 kcal.mol^{-1} and 2.47 μM, respectively as shown in Table 2 and Fig. 4. One hydrogen bond has been formed from atoms on ligand to active sites of amino acids of a target protein of 7KCD. They named D:Leu 462: N – FLV1:O (2.99 Å) and was one hydrophilic interaction. Ranked pose 35 showed well ligand interactions because it included 3 parts (capping group- identification of protein, connecting unit (CU) or linker, and functional group) have fully interactions

(Dokmanovic et al., 2007). For capping group of pose 35, it detected aromatic ring or heterocyclic via one amide pi-stacked from Leu 429: C chain to pi electrons of aromatic ring, alkyl or pi-alkyl ligand interactions from Ala 430 of C chain, one pi cation – one electrostatic interaction from Lys 472: D chain to pi electrons of another aromatic ring, and alkyl or pi-alkyl from Arg 434 and Ser 433: C chain to aromatic ring of this pose. Linker of pose 35 was detected via one hydrophobic interaction from Leu 429: C chain to methyl of methoxy group on this pose. Finally, functional group of pose 35 was identified by one hydrogen bonding from Asp 426: C chain to hydrogen atom of phenolic hydroxyl group and one pi alkyl or alkyl from Leu 429: C chain to methyl of methoxy group of aromatic ring. Pose 375, ligand FLV-2, ranked pose among 400 poses
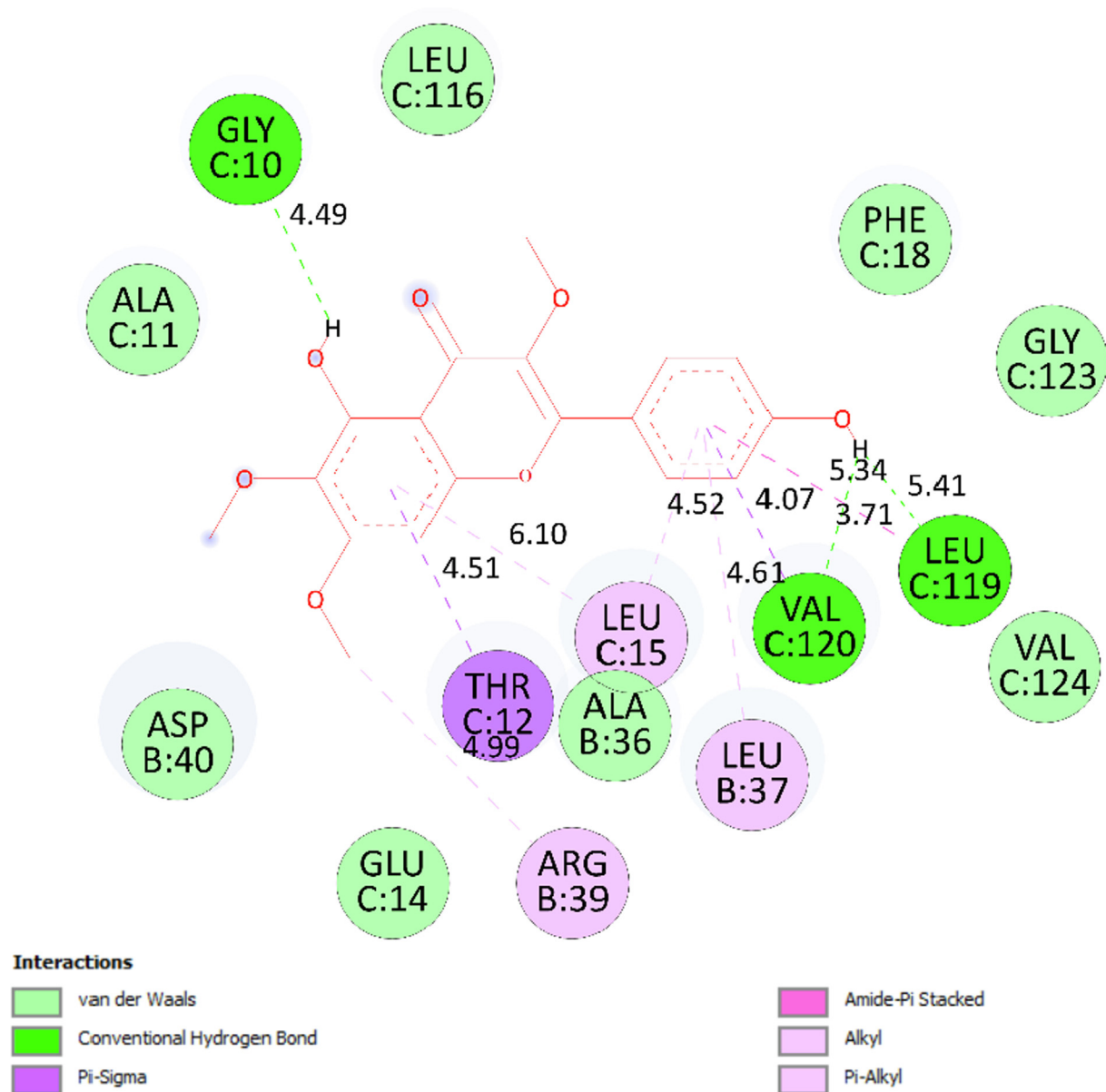
Fig. 11. Pose 238, one ranked pose of ligand FLV-3 was docked to **2G33: PDB.**

docked to 7KCD with the values of ΔG^o and Ki of −66 Kcal mol⁻¹ and 14.55 μM, respectively, as shown in Table 2. It formed two hydrogen bonding with active atoms on 7KCD, as seen in Table 2. The significant ligand interactions between pose 88 and 7KCD indicated in Fig. 5. Ligand FLV-2 or pose 375 was identified good ligand interaction because 3 parts of pose 375 interacted well with receptor 7KCD. Those ligand interactions identified pi-amide stacked: Leu 429, Ser 433, pi-cation: Lys 472, pi-alkyl or alkyl: Ala 430, His 476, Arg 434, and hydrogen bonding: Asp 426 and His 476. Pose 23, ligand FLV-3 and DOX also detected good ligand interactions as analysis analogues. The ranked model of ligand interactions and thermodynamic site was DOX (pose 139) > FLV-2 (pose 375) > FLV-1 (Pose 35) > FLV-3.

The validations of interaction model between ligand and receptor, 7KCD were further investigated. As shown Table 3 and Fig. 8, the values of pair poses are calculated by reference pose 375. The

values of pair poses of ligand FVL-1 to FLV3 after completing docking calculations are listed by (pose 35, pose 375) of 0.015 Å, (pose 23, pose 375) of 0.401 Å, and (pose 139, pose 375) of 0.401 Å. All the values of RMSD of pair poses are lower than 2 Å, which confirmed the validations of molecular docking model in silico about docking parameter, relocking, orientation docking, in processing of docking and allowed to obtain the good predict of interesting compound in biochemistry and drug discovery recently (Hidalgo-Figueroa et al., 2021).

In addition, docking of ligand FLV-1 to FLV-3 and drug, DOX to receptor 2G33 was confirmed. The role ligand interactions and the validations of model of ligand FLV-1 to FLV-3 and DOX to receptor 2G33 indicated in Table 2-3 and Figs. 10-13. As indicated in Table 2, ranked poses of ligand FLV1 or ranked pose 85, ligand FLV-2 or ranked pose 88, ligand FLV-3 or pose 238, and ligand DOX or pose 176 exposed the values as ΔG^o,
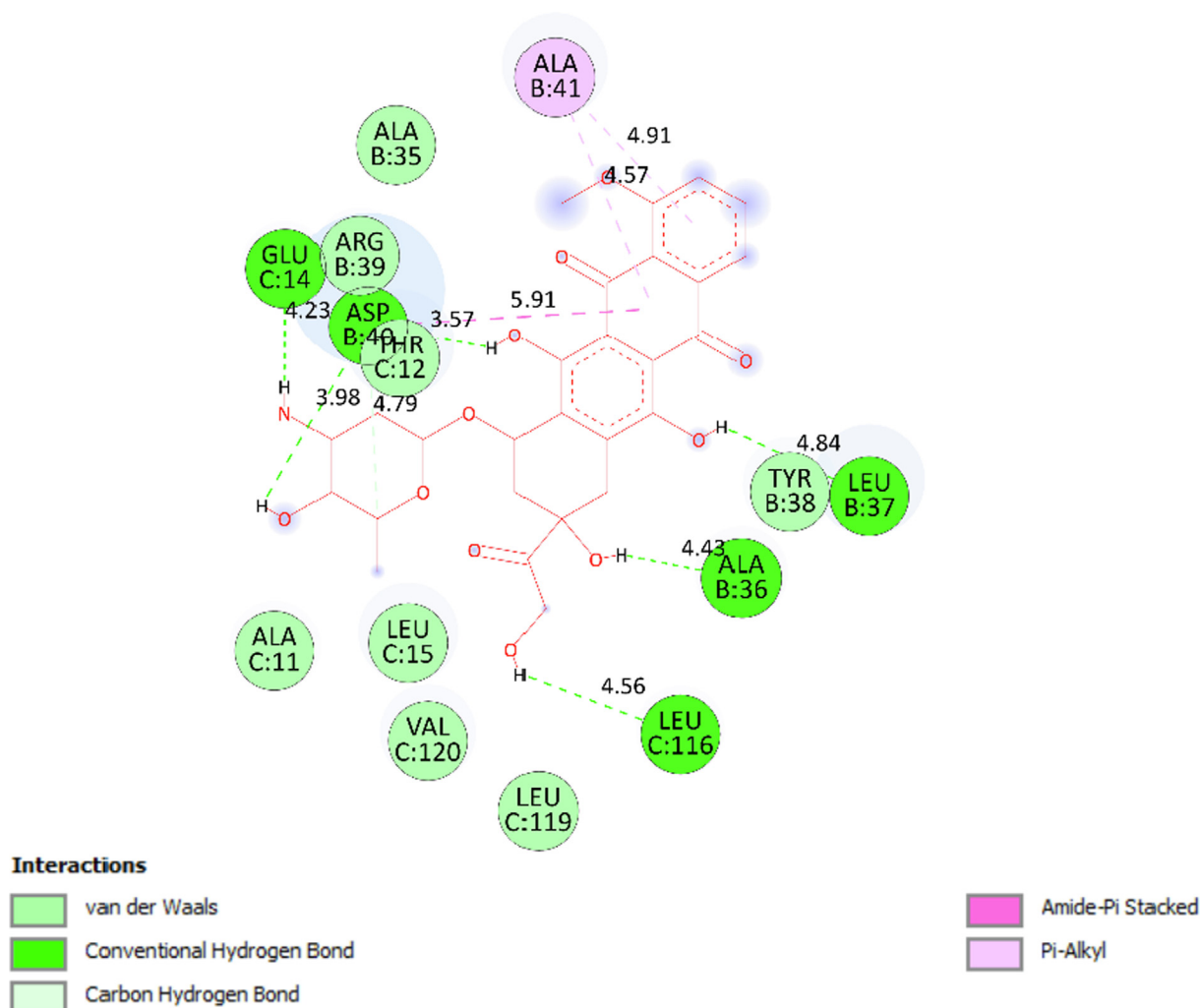
Interactions

(light green)	van der Waals
(green)	Conventional Hydrogen Bond
(pale green)	Carbon Hydrogen Bond
(magenta)	Amide-Pi Stacked
(pink)	Pi-Alkyl

Fig. 12. Pose 176, one ranked pose of ligand DOX was docked to **2G33: PDB.**

Ki, the number of hydrogen characters. At thermodynamic site, the ranked poses exposed by pose 176 (DOX) > pose 238 (FLV-3) > pose 85 (FLV-1) > pose 88 (FLV-2). The analysis of ligand interactions of ranked poses with target protein, 2G33 indicated the active poses in order to 176 (DOX) > pose 238 (FLV-3) > pose 85 (FLV-1) > pose 88 (FLV-2). For ligand, ligand FLV-3 or pose 238 are the best pose docking among candidate for docking to receptor 2G33.

The validations of interaction model between ligand and receptor, 2G33. As shown Table 4 and Fig. 13. As seen in Table 4 the values of RMSD of pair poses calculated by PyMOL software in this case reference pose 238 (ligand FLV-3). The values of pair poses were (pose 85, pose 238) of 0.028 Å, (pose 88, pose 238) of 0.011, (pose 176, pose 176) of 3.505 Å. The values of RMSD between poses of ligand FLV-1 to FLV-3 were lower than 2 Å and proved the validation of in silico docking model in docking parameter which are sued in docking calculations, active center on receptor, docking orientation, docking processing and allowed us to predict good interactions with interesting ligand. Other pair poses, the values of RMSD exposed the changes of conformation before docking and after completing docking of the same ligand, for instance, (pose FLV-1, pose 35) of 4.126 Å, which proved that ligand FLV-1 was large change in conformation of it after completing docking.
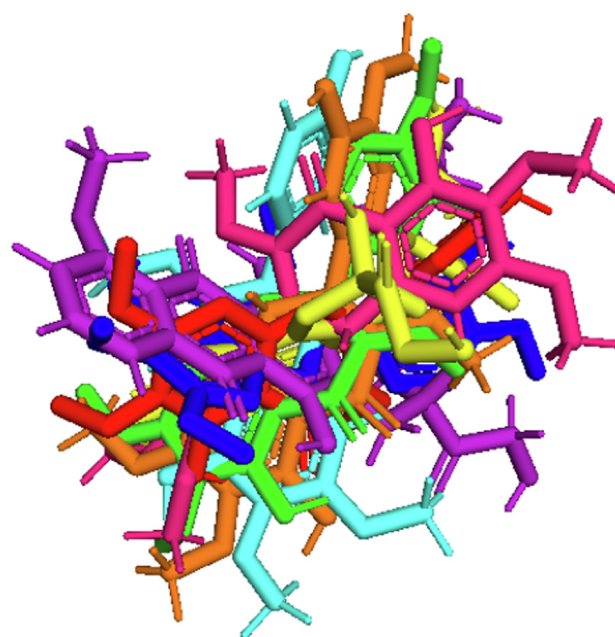

Fig. 13. Pose 88 (blue color), Pose 85 (green color), pose 176 (yellow color), FLV-1 (magenta color), FLV-2 (orange color), FLV-3 (cyan color), and DOX (Purpose color) are aligned to Pose 238 (red color), one reference pose.

Table 2
The significant results have obtained from molecular docking model of ligand and drug, DOX to receptor 7KCD and 2G33: PDB.

Entry	Ranked pose	Free Energy of Binding[a]	K[b]	The number of hydrogen bonds[c]	The property and bond length[d]
7KCD: PDB					
FLV − 1	35	−7.71	2.24	1	D:Leu 462:N – FLV1:O (2.99 Å)
FLV − 2	375	−7.12	6.07	2	D:Leu 462:N – FLV–2:O (2.89 Å)
					FLV–2:H – C:Asp 426:O (2.36 Å)
FLV − 3	23	−6.88	9.11	2	A:Lys 472:N – FLV − 3:O (2.65 Å)
					FLV − 3:H - B:Ala430:O (1.84 Å)
DOX	139	−8.65	0.459	5	A:Arg477:N– DOX:N (3.18 Å)
					B:Arg434:N–DOX:O (2.80 Å)
					DOX:H–A:Asp473:O (2.20 Å)
					DOX:H–A:Asp473:O (2.36 Å)
					DOX:H–A:Leu469:O (1.88 Å)
2G33: PDB					
FLV − 1	85	−6.62	13.96	3	C:Ala 11:N – FLV − 1:O (3.18 Å)
					C:Va l120:N – FLV − 1:O (2.92 Å)
					FLV − 1:H – C:Gly 10:O (2.31 Å)
FLV − 2	88	−6.60	14.55	2	C:Ala 11:N – FLV − 2:O (3.12 Å)
					FLV − 2:H – C:Gly 10:O (2.34 Å)
FV − 3	238	−7.60	2.67	1	FLV − 3:H – C:Val120:O (2.18 Å)
DOX	176	−8.22	0.943	5	DOX:H − B:Asp 40:O (2.07 Å)
					DOX:H − C:Glu 14:O (2.30 Å)
					DOX:H − C:Glu 14:O (1.64 Å)
					DOX:H − B:Asp 40:O (2.04 Å)
					DOX:H − B:Ala 36:O (2.11 Å)

[a]. They have done by AutoDockTools−1.5.6rc3 package in unit of kcal.mol^{-1}. [b]. The K_i have obtained in unit of μM via AutoDockTools−1.5.6rc3 package. [c], [d]. They have built based on Discovery Studio (DSC) package.

Table 3
The values of RMSD of pair poses docked to 7KCD: PDB and calculated by PyMOL software.

RMSD, Å	FLV-1	FLV-2	FLV-3	DOX	Pose 35	Pose 375	Pose 23	Pose 139
FLV-1	0	5.520	5.921	6.837	4.126	3.433	1.478	4.660
FLV-2	5.520	0	3.661	6.313	1.884	4.195	4.453	3.734
FLV-3	4.195	3.661	0	5.614	5.150	5.204	5.150	3.416
DOX	6.837	6.313	5.614	0	1.826	1.933	1.769	2.613
Pose 35	4.126	1.884	5.150	1.826	0	0.015	0.365	3.286
Pose 375	3.433	4.195	5.204	1.933	0.015	0	0.401	3.443
Pose 23	1.478	4.453	5.150	1.769	0.365	0.401	0	3.574
Pose 139	4.66	3.734	3.416	2.613	3.286	0.401	3.574	0

Table 4
The values of RMSD of pair poses docked to 2G33: PDB and calculated by PyMOL software.

RMSD, Å	FLV-1	FLV-2	FLV-3	DOX	Pose 85	Pose 88	Pose 238	Pose 176
FLV-1	0	5.520	5.921	6.837	3.20	2.422	2.310	4.771
FLV-2	5.520	0	3.661	6.313	2.430	5.507	4.192	4.107
FLV-3	5.921	3.661	0	5.614	5.168	5.167	5.061	4.283
DOX	6.837	6.313	5.614	0	1.817	2.012	1.858	2.819
Pose 85	3.20	2.430	5.168	1.817	0	0.019	0.028	3.281
Pose 88	2.422	5.507	5.167	2.012	0.019	0	0.011	2.818
Pose 238	2.310	4.192	5.061	1.858	0.028	0.011	0	3.505
Pose 176	4.771	4.107	4.283	2.819	3.281	2.818	3.505	0

5. Conclusion

In conclusion, our findings suggest that FLV1, FLV2, and FLV3 have signifcant in vitro antitumor selective activity against human breast and liver cancer cells, HepG2 and MCF-7, inducing cell death by an apoptotic mechanism involving caspases activity and DNA fragmentation. However, in terms of the IC50 profiles obtained with those compounds, FLV1 and FLV3 demonstrated to be more potent antitumor agents than FLV2. It is important to note that to confirm these in vitro and our docking studies revealed the compounds are the best candidates docked to 7KCD and 2G33, involved in the generation of cellular death through extrinsic or intrinsic pathways. Additionally, it would be very interesting to further evaluate the antiproliferative activity of FLV1, FLV2, and FLV3 on other cancer cell lines. Finally, in silico and in vitro predictions of physicochemical properties, toxicities, and pharmacokinetics revealed that studies on the anti-cancer activity of artemetin, vitexicarpin and penduletin compounds should be taken into consideration as good anticancer candidates for further study.

Declaration of Competing Interest

The authors declare that they have no known competing financial interests or personal relationships that could have appeared to influence the work reported in this paper.

Acknowledgments

Appendix A. Supplementary material

Supplementary data to this article can be found online at https://doi.org/10.1016/j.jsps.2022.06.018.

References

An, T.N.M., Cuong, N.V., Quang, N.M., Thanh, T.V., Alam, M., 2020. Green synthesis using PEG-400 catalyst, antimicrobial activities, cytotoxicity and in silico molecular docking of new carbazole based on α-aminophosphonate. ChemistrySelect 5 (21), 6339–6349. https://doi.org/10.1002/slct.202000855.

Azhar Ul, H., Malik, A., Anis, I., et al., 2004. Enzyme inhibiting lignans from Vitex negundo. Chem. Pharm. Bull. 52, 1269–1272. https://doi.org/10.1248/cpb.52.1269.

Bell, E.W., Zhang, Y., 2019. DockRMSD: an open-source tool for atom mapping and RMSD calculation of symmetric molecules through graph isomorphism. J. Cheminf. 11, 40. https://doi.org/10.1186/s13321-019-0362-7.

Brentnall, M., Rodriguez-Menocal, L., De Guevara, R.L., Cepero, E., Boise, L.H., 2013. Caspase-9, caspase-3 and caspase-7 have distinct roles during intrinsic apoptosis. BMC Cell Biol. 14 (1). https://doi.org/10.1186/1471-2121-14-32.

Couffignal, A.L., Lapeyre-Mestre, M., Bonhomme, C., et al., 2000. Adverse effects of anticancer drugs: apropos of a pharmacovigilance study at a specialized oncology institution. Therapie 55, 635–641.

Cragg, G.M., Newman, D.J., 2013. Natural products: a continuing source of novel drug leads. Biochim. Biophys. Acta 1830 (6), 3670–3695. https://doi.org/10.1016/j.bbagen.2013.02.008.

Cragg, G.M., Pezzuto, J.M., 2016. Natural products as a vital source for the discovery of cancer chemotherapeutic and chemopreventive agents. Med. Principles Pract. 25 (suppl 2), 41–59. https://doi.org/10.1159/000443404.

Desai, A.G., Qazi, G.N., Ganju, R.K., et al., 2008. Medicinal plants and cancer chemoprevention. Curr. Drug Metab. 9, 581–591. https://doi.org/10.2174/138920008785821657.

Díaz, F., Chávez, D., Lee, D., Mi, Q., Chai, H.-B., Tan, G.T., Kardono, L.B.S., Riswan, S., Fairchild, C.R., Wild, R., Farnsworth, N.R., Cordell, G.A., Pezzuto, J.M., Kinghorn, A.D., 2003. Cytotoxic flavone analogues of vitexicarpin, a constituent of the leaves of Vitex negundo. J. Nat. Prod. 66 (6), 865–867. https://doi.org/10.1021/np0300784.

Dokmanovic, M., C. Clarke and P. A. Marks, 2007. Histone deacetylase inhibitors: overview and perspectives. Molecular cancer research : MCR. 5, 981-989. https://doi.org/10.1158/1541-7786.mcr-07-0324.

Duong, T.-H., X.-H. Bui, P. Le Pogam, et al., 2017. Two novel diterpenes from the roots of Phyllanthus acidus (L.) Skeel. Tetrahedron. 73, 5634-5638. https://doi.org/https://doi.org/10.1016/j.tet.2017.07.021.

Duong, T.-H., Paramita Devi, A., Tran, N.-M.-A., Phan, H.-V.-T., Huynh, N.-V., Sichaem, J., Tran, H.-D., Alam, M., Nguyen, T.-P., Nguyen, H.-H., Chavasiri, W., Nguyen, T.-C., 2020. Synthesis, α-glucosidase inhibition, and molecular docking studies of novel N-substituted hydrazide derivatives of atranorin as antidiabetic agents. Bioorg. Med. Chem. Lett. 30 (17), 127359. https://doi.org/10.1016/j.bmcl.2020.127359.

Enkhtaivan, G., D. H. Kim and M. Pandurangan, 2017. Cytotoxic effect of TDZ on human cervical cancer cells. Journal of photochemistry and photobiology. B, Biology. 173, 493-498. https://doi.org/10.1016/j.jphotobiol.2017.06.032.

Fulda, S., Debatin, K.-M., 2006. Extrinsic versus intrinsic apoptosis pathways in anticancer chemotherapy. Oncogene 25 (34), 4798–4811. https://doi.org/10.1038/sj.onc.1209608.

Gautam, L., Shrestha, S., Wagle, P., et al., 2010. Chemical constituents from Vitex negundo (Linn.) of Nepalese origin. Scientific World 6, 27–32.

Goldin, A., Venditti, J.M., Macdonald, J.S., Muggia, F.M., Henney, J.E., Devita, V.T., 1981. Current results of the screening program at the division of cancer treatment, national cancer institute. Eur. J. Cancer 17 (2), 129–142. https://doi.org/10.1016/0014-2964(81)90027-x.

Grever, M.R., Schepartz, S.A., Chabner, B.A., 1992. The national cancer institute: cancer drug discovery and development program. Semin. Oncol. 19, 622–638.

Harvey, A.L., Edrada-Ebel, R., Quinn, R.J., 2015. The re-emergence of natural products for drug discovery in the genomics era. Nat. Rev. Drug Discovery 14 (2), 111–129. https://doi.org/10.1038/nrd4510.

Hidalgo-Figueroa, S., Rodríguez-Luévano, A., Almanza-Pérez, J.C., Giacoman-Martínez, A., Ortiz-Andrade, R., León-Rivera, I., Navarrete-Vázquez, G., 2021. Synthesis, molecular docking, dynamic simulation and pharmacological characterization of potent multifunctional agent (dual GPR40-PPARγ agonist) for the treatment of experimental type 2 diabetes. Eur. J. Pharmacol. 907, 174244. https://doi.org/10.1016/j.ejphar.2021.174244.

Kadir, F.A., Kassim, N.M., Abdulla, M.A., et al., 2013. PASS-predicted Vitex negundo activity: antioxidant and antiproliferative properties on human hepatoma cells–an in vitro study. BMC Complement Altern. Med. 13, 343. https://doi.org/10.1186/1472-6882-13-343.

Kumar, M., Kaur, P., Kumar, S., Kaur, S., 2015. Antiproliferative and apoptosis inducing effects of non-polar fractions from Lawsonia inermis L. in cervical (HeLa) cancer cells. Physiol. Mol. Biol. Plants : Int. J. Funct. Plant Biol. 21 (2), 249–260. https://doi.org/10.1007/s12298-015-0285-3.

Li, W.-X., Cui, C.-B., Cai, B., Wang, H.-Y., Yao, X.-S., 2005. Flavonoids from Vitex trifolia L. inhibit cell cycle progression at G2/M phase and induce apoptosis in mammalian cancer cells. J. Asian Nat. Prod. Res. 7 (4), 615–626. https://doi.org/10.1080/10286020310001625085.

Newman, D.J., Cragg, G.M., 2016. Natural Products as Sources of New Drugs from 1981 to 2014. J. Nat. Prod. 79 (3), 629–661. https://doi.org/10.1021/acs.jnatprod.5b01055.

Nguyen, N.H., Nguyen, T.T., Ma, P.C., Ta, Q.T.H., Duong, T.-H., Vo, V.G., 2020. Potential antimicrobial and anticancer activities of an ethanol extract from Bouea macrophylla. Molecules (Basel, Switzerland) 25 (8), 1996. https://doi.org/10.3390/molecules25081996.

Postiglione, A.E., Muday, G.K., 2020. The role of ROS homeostasis in ABA-induced guard cell signaling. Front. Plant Sci. 11. https://doi.org/10.3389/fpls.2020.00968.

Rajora, A.K., Ravishankar, D., Zhang, H., Rosenholm, J.M., 2020. Recent advances and impact of chemotherapeutic and antiangiogenic nanoformulations for combination cancer therapy. Pharmaceutics 12 (6), 592. https://doi.org/10.3390/pharmaceutics12060592.

Rani, A., Sharma, A., 2013. The genus Vitex: a review. Pharmacogn. Rev. 7, 188–198. https://doi.org/10.4103/0973-7847.120522.

Sathiamoorthy, B., Gupta, P., Kumar, M., Chaturvedi, A.K., Shukla, P.K., Maurya, R., 2007. New antifungal flavonoid glycoside from Vitex negundo. Bioorg. Med. Chem. Lett. 17 (1), 239–242. https://doi.org/10.1016/j.bmcl.2006.09.051.

Shaker, G.H., Melake, N.A., 2012. Use of the single cell gel electrophoresis (comet assay) for comparing apoptotic effect of conventional antibodies versus nanobodies. Saudi Pharma. J. 20, 221–227. https://doi.org/10.1016/j.jsps.2011.11.004.

Sharma, R.L., Prabhakar, A., Dhar, K.L., Sachar, A., 2009. A new iridoid glycoside from Vitex negundo Linn (Verbenacea). Nat. Prod. Res. 23 (13), 1201–1209. https://doi.org/10.1080/14786410802696494.

Sibanyoni, M.N., Chaudhary, S.K., Chen, W., Adhami, H.-R., Combrinck, S., Maharaj, V., Schuster, D., Viljoen, A., 2020. Isolation, in vitro evaluation and molecular docking of acetylcholinesterase inhibitors from South African Amaryllidaceae. Fitoterapia 146, 104650. https://doi.org/10.1016/j.fitote.2020.104650.

Sichaem, J., Nguyen, H.-H., Nguyen, V.-H., Mac, D.-H., Mai, D.-T., Nguyen, H.-C., Tran, T.-N.-M., Pham, N.-K.-T., Nguyen, H.-H., Niamnont, N., Duong, T.-H., 2019. A new labdane-type diterpenoid from the leaves of Vitex negundo L. Nat. Prod. Res. 35 (14), 2329–2334. https://doi.org/10.1080/14786419.2019.1672687.

Siegel, R.L., Miller, K.D., Fuchs, H.E., Jemal, A., 2022. Cancer statistics. CA: Cancer J. Clin. 72 (1), 7–33. https://doi.org/10.3322/caac.21708.

Sung, H., Ferlay, J., Siegel, R.L., Laversanne, M., Soerjomataram, I., Jemal, A., Bray, F., 2021. Global cancer statistics 2020: GLOBOCAN estimates of incidence and mortality worldwide for 36 cancers in 185 Countries. CA Cancer J. Clin. 71 (3), 209–249. https://doi.org/10.3322/caac.21660.

Wu, Y., Zhao, D., Zhuang, J., Zhang, F., Xu, C., Gallyas, F., 2016. Caspase-8 and caspase-9 functioned differently at different stages of the cyclic stretch-induced apoptosis in human periodontal ligament cells. PLoS One 11 (12), e0168268. https://doi.org/10.1371/journal.pone.0168268.

Zheng, C.-J., Huang, B.-K., Han, T., Zhang, Q.-Y., Zhang, H., Rahman, K., Qin, L.-P., 2009. Nitric oxide scavenging lignans from Vitex negundo seeds. J. Nat. Prod. 72 (9), 1627–1630. https://doi.org/10.1021/np900320e.

Zheng, C.-J., Huang, B.-K., Wang, Y., Ye, Q.i., Han, T., Zhang, Q.-Y., Zhang, H., Qin, L.-P., 2010. Anti-inflammatory diterpenes from the seeds of Vitex negundo. Bioorg. Med. Chem. 18 (1), 175–181. https://doi.org/10.1016/j.bmc.2009.11.004.